Study of Riprap as Scour Protection for Spill-Through Abutments

A. TAMIM ATAYEE

The purpose of the study was to develop empirical design guidelines for riprap protection of spill-through abutments situated in floodplains near channels. Previous laboratory studies have been done for a simple prismatic cross section with spill-through abutments encroaching less than 56 percent of the floodplain width. Previous studies are extended through an experiment with compound channels consisting of a floodplain and a defined main channel encompassing encroachments ranging from 62 to 100 percent of the floodplain. With the benefit of physical models, empirical design guidelines for the protection of spill-through abutments are provided for the broad range of abutment and floodplain configurations. Previous laboratory experiments have been done using the depth-averaged measured approach velocity and Bernoulli's conservation of energy equation to approximate the average contracted velocity. The average contracted velocity is the controlling variable to compute the design grain size, D_{50}, of the riprap. The experiments extend the range of encroachment from 56 to 100 percent of the floodplain width in a physical model composed of a channel, a floodplain, spill-through abutments of various lengths, and riprap (gravel) of various grain sizes. Data from previous laboratory experiments and the current study were used to develop an empirical relationship to size riprap to protect abutments.

Construction of structures within floodplains has significant effects on the hydraulic performance of a stream. These effects are even more pronounced during floods when the majority of the flood flow is in the floodplain overbanks rather than the natural channel. Encroachments onto the floodplain tend to have a contraction effect on the unobstructed approach flow. By introducing an obstruction in the floodplain, the natural flow area is decreased, thus increasing the average velocity.

Obstruction of flows by bridge substructures, such as embankments, abutments, and piers, redirects the natural course of the stream and in doing so accelerates flow and disrupts the streamlines. Residual secondary currents—specifically, vortices and flow separation—are the result. These vortices are rotational currents whose potential to erode the alluvial stream bed increases as the currents grow stronger. The base of the bridge substructures is the most susceptible place for local scour to occur. The unprotected stream bed can experience enough sediment removal to form a scour hole that could potentially undermine the foundation of the bridge substructure. Furthermore, the transport of larger sediment particles impinges the bridge substructures, chips away at the concrete, and poses a threat to the composition of the member. These contributing hydraulic factors that precipitate the scouring at bridge foundations are the leading cause for the bridge failures over streams and rivers.

GKY and Associates, Inc., 5411-E Backlick Road, Springfield, Va. 22151.

COUNTERMEASURES

There are several countermeasures for mitigating local scour caused by encroachment into waterways: for example, relief openings in the bridge substructure, guide banks (spur dikes), channel improvement, and riprap revetment. Rock riprap revetment provides an effective measure to protect streams from the destructive effects of scour. To determine the amount of riprap necessary to adequately protect abutments, the scour potential must be known. The scour potential can be determined if the stream hydraulic characteristics, such as depth and velocity, are known. To dissipate energy effectively, thereby providing erosion protection, the appropriate median grain size and proper gradation and implementation must be employed. Moreover, the particle should be resistant to weathering that may be due to fluid forces, exposure, and abrasion from contact with other particles. One of the goals of this study is to provide a method for determining the appropriate size of riprap for a specified flow condition.

LITERATURE REVIEW

The initiation or threshold of movement of a particle due to the action of fluid flow is defined as the instant when the applied forces due to fluid drag and lift, causing the particle to move, and exceed the stabilizing force due to the particle weight force (*1*). This hydraulic condition is known as incipient motion and the acting forces are depicted in Figure 1, in which L = lift force, W = particle weight, F_D = drag force, F_R = resisting force, and α = angle of contact. These forces are the prevalent forces for grains of noncohesive sediment lying in a bed of similar grains over which fluid is flowing (*2*). The grain is subjected to fluid forces that promote movement and gravitational forces that resist movement. In the presence of these forces, a shear stress forms between the grains on the threshold of motion and the stable grains that compose the stationary boundary.

DIMENSIONAL ANALYSIS

To understand the nature of scour, the mathematical principles describing the bed geometry, capacity, and supply as functions of flow conditions and time must be established.

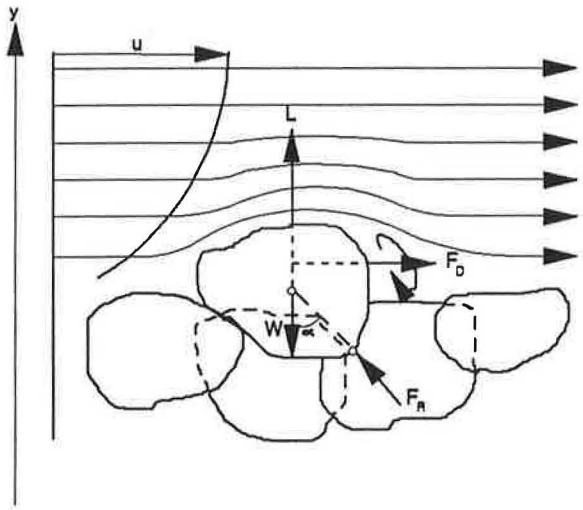

FIGURE 1 Schematic of particle and fluid forces (2).

The following relation describes the contributing factors in the erosion, transport, and deposition of sediment associated with local scour (2):

$$f(B) = \phi_1[g(B),g(S),t] \tag{1}$$

where

$f(B)$ = mathematical description of boundary,
t = time,
$g(B)$ = sediment discharge or transport rate out of scour zone as function of boundary shape and position, and
$g(S)$ = rate of supply to scour zone.

In the absence of the aforementioned mathematical principles, the emphasis must be placed on experiments to determine the functions empirically. After dimensional analysis the bed configuration function becomes a function of average and shear velocities, Reynolds number, and Froude number (2):

$$f(B) = \left[\frac{V}{\sqrt{\frac{\tau_c}{\rho}}}, \sigma, \frac{Vt}{a}, \frac{Va}{\nu}, \frac{V^2}{ga}, \frac{b}{a}, g(S)\right] \tag{2}$$

where

τ_c = critical tractive force for sediment composing bed,
ρ = fluid density,
σ = standard deviation of particle size distribution,
a = characteristic length describing size of system,
ν = kinematic viscosity of fluid,
b = typical length of flow pattern,
V = velocity, and
g = gravitational acceleration.

The use of noncohesive sediments in laboratory studies has been justified as documented by Vanoni:

> Aside from numerous experiments relating to land erosion, the generalized study of scour by flowing water has been limited to studies involving noncohesive soils. Although the property of cohesiveness is of paramount importance in such scour phenomena occurring below conservation and control structures, in bank caving of streams, and in the design of artificial channels constructed in cohesive materials, there are also many problems involving scour of noncohesive soils, e.g., bed scour in natural streams and scour around bridge piers and downstream of outlet works. In addition, considerable progress has been made in the design of stuctures discharging on cohesive soils through model studies using noncohesive sediments. (2)

These experiments are characterized by fully turbulent flow in which the Reynolds number becomes very high (on the order of 10^4 or greater). Since the physical modeling involved only clear-water scour experiments, uniformly graded gravel, and noncohesive soil, and because the experiment was conducted under steady-state conditions, the equation simplifies to a function of relative shear velocity, Froude number, and a dimensionless length ratio:

$$f(B) = \left[\frac{V}{\sqrt{\frac{\tau_c}{\rho}}}, \frac{V^2}{ga}, \frac{b}{a}\right] \tag{3}$$

The length ratio, b/a, has been commonly represented by the relative roughness, D_{50}/y, in scour studies. There exists a relationship between the sediment number, N_{sc}, and the relative roughness. If this relationship is known, a solution for the riprap size, D_{50}, can be achieved. The other hydraulic identities of interest, in the context of this study, derived from dimensional analysis are Shields parameter, sediment number, and Froude number.

SHIELDS PARAMETER

The Shields parameter is a dimensionless hydraulic identity equal to the ratio of the kinematic forces that influence particle motion to the gravitational forces that resist movement (3). This property is a quantitative indication of particle stability. The shear stress due to the kinematic forces of the fluid can be defined by the following equation:

$$\tau_o = \gamma\, d\, S_e = \rho\, u_*^2 \tag{4}$$

where

γ = specific weight of water [N/m³ (lb/ft³)],
d = flow depth [m (ft)],
S_e = energy slope,
ρ = density of water [kg/m³ (slug/ft³)], and
u_* = $(g\, y\, S_e)^{0.5}$
= shear velocity [m/sec (ft/sec)].

The shear stress of the particle to resist movement is represented by the following equation:

$$\tau = \rho g(S_g - 1)D_{50} \tag{5}$$

The Shields parameter, or the critical dimensionless shear stress, is therefore defined as Equation 4 divided by Equation 5:

$$\tau_* = \frac{dS_e}{D_{50}(S_b - 1)} = \frac{u_*^2}{g(S_g - 1)D_{50}} \quad (6)$$

SEDIMENT NUMBER

Like the Shields parameter, the sediment number, N_{sc}, is a ratio of the shear stress due to fluid forces to the shear stress of the particle to resist movement. Furthermore, this property is also an indicator of particle stability. However, the difference between the two stability parameters is that the sediment number is a velocity-based criterion whereas the Shields parameter is a shear stress–based criterion. Hence, the numerator term that defines the fluid shear stress is a function of velocity.

Isbash defined the stability of noncohesive particles on the basis of average velocity criteria. An empirical dimensionless coefficient, E, was determined for the particles (*4*). The sediment number is related to this coefficient as depicted in the following equation:

$$N_{sc} = 2E^2 \quad (7)$$

For loose stones lying on top of other stones, $E = 0.86$, and for stones "seated" among the other stones, $E = 1.20$ (*4*). The higher coefficient value for seated stones than for loose stones reflects the particles' potential to be more resistant to movement. Hence, a higher velocity is associated with the more stable particle. By substituting an average velocity for the shear velocity in Equation 4, the shear stress due to kinematic forces of the fluid as a function of velocity can be defined as

$$\tau_o = \rho V^2 \quad (8)$$

The equation for the sediment number becomes a ratio of Equation 8 to Equation 5:

$$N_{sc} = \frac{V^2}{g(S_g - 1)D_{50}} \quad (9)$$

Comparing Equations 6 and 9 demonstrates the similarities between Shields parameter and the sediment number. These are the two parameters that have historically been used to evaluate incipient motion for sediment in water.

FROUDE NUMBER

The Froude number is a hydraulic identity that is the ratio of the inertial to gravitational forces. This dimensionless property is a disruptive term for the flow field acting on the particles. In this study, the Froude number is a function of the spatially averaged velocity and depth as defined by the following equation:

$$\mathrm{Fr} = \frac{V}{\sqrt{gd}} \quad (10)$$

where Fr is the Froude number.

RELATED LABORATORY EXPERIMENTS

In 1990 laboratory experiments were conducted in the FHWA Hydraulics Laboratory tilting flume to determine the stability of rock riprap protecting abutments in floodplains (*5*). The abutment models were represented by two different shapes: a vertical and a spill-through abutment. These experiments yielded extensive measured data that could be used to interpret the behavior of sediment relative to the prevailing hydraulic characteristics. The results were presented as a relationship between sediment number, N_{sc}, and relative roughness, D_{50}/d_{cc} as depicted in Figure 2. Figure 2 is an illustration of calculated sediment number and calculated relative roughness. The velocity term in Equation 9 is represented by a calculated average constricted velocity, V_{cc}. The relative roughness flow depth term, d_{cc}, is a calculated value along with V_{cc} determined by satisfying the energy equation from the approach section to the constricted section of the laboratory model.

RIPRAP AS COUNTERMEASURE AGAINST SCOUR

Studies have been done to provide rock riprap design guidelines for protecting bridge abutments from erosion. FHWA published design criteria in *Design of Riprap Revetment*, Hydraulic Engineering Circular (HEC) 11 (*6*), which recommends that a rock riprap layer should be extended at least 1.52 m (5 ft) below the stream bed and on a continuous slope with the channel embankment. The design equation for sizing riprap as protection for channels and bridge abutments, as recommended in HEC-11, can be presented in the following form:

$$D_{50} = \left(\frac{0.001\ V_a^3}{d_{\mathrm{avg}}^{0.5}\ K_1^{1.5}}\right) C_{sg} C_{sf} C_{P/A} \quad (11)$$

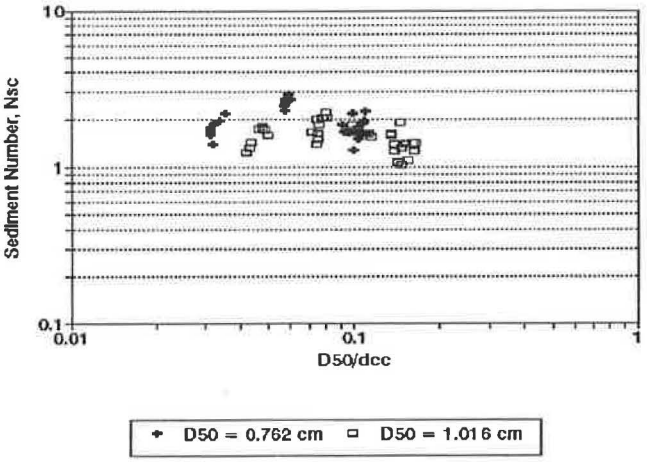

FIGURE 2 Relationship between sediment number and relative roughness for spill-through abutment on floodplain with no channel.

where

V_a = average velocity in main channel (ft/sec),
d_{avg} = average depth in main channel (ft),
K_1 = $\{1 - (\sin^2 \theta / \sin^2 \phi]\}^{0.5}$,
θ = bank angle with horizontal,
ϕ = riprap particle's angle of repose,
C_{sf} = correction factor for stability factor,
C_{sg} = correction factor for specific gravity, and
$C_{P/A}$ = correction factor to account for acceleration of velocities when flow is obstructed by piers or abutments.

In the context of this paper, Equation 11 can apply to the design of riprap on the floodplain and the channel. Since Equation 11 defines D_{50} with a specific gravity of 2.65 and stability factor of 1.2, the following correction factors must be multiplied with Equation 11 to obtain the stable riprap size for different S_g and SF values:

$$C_{sg} = \frac{2.12}{(S_g - 1)^{1.5}} \tag{12}$$

$$C_{sf} = \left(\frac{SF}{1.2}\right)^{1.5} \tag{13}$$

where SF is the stability factor, and $C_{P/A} = (1.5)^3 = 3.38$. HEC-11 recommends that stability factor range of 1.6 to 2.0 should apply for riprap design in the vicinity of bridge abutments (*6*). This criteria in HEC-11 was published as an interim procedure to be used until better criteria could be developed.

Currently, the design equation for sizing riprap for pier protection is a rearranged form of the Isbash equation. Applying the seated dimensionless coefficient to Equation 9 yields the following equation:

$$D_{50} = \frac{0.347\ V^2}{g(S_g - 1)} \tag{14}$$

The Isbash equation has been modified for spill-through abutments on the basis of an experimental study. Previous spill-through abutment laboratory experiments have yielded a design equation for determining stable riprap size (*5*):

$$D_{50} = \frac{0.535\ V_{cc}^2}{g\ (S_g - 1)} \tag{15}$$

where V_{cc} is the computed average velocity at the contraction within the floodplain, in feet per second.

Equation 15 is derived from a relationship between the sediment number and the relative roughness, D_{50}/y. The velocity term is a computed value based on the energy equation applied to the approach and constricted sections.

DESCRIPTION OF EXPERIMENTAL SETUP FOR CURRENT STUDY

The physical scale model is comprised of a spill-through abutment, a floodplain, a channel and a gravel apron. The model was not site-specific, so a scaling ratio is not applicable, but generally, model length dimensions were about 1/50th of the typical prototype dimensions. Figure 3 illustrates a plan view of the physical model.

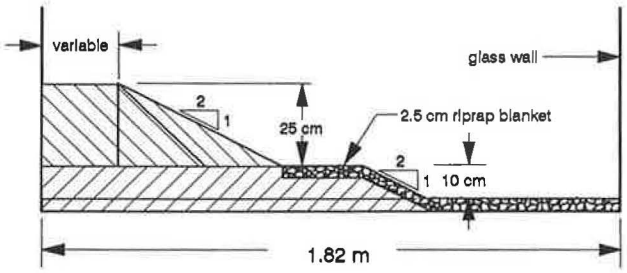

FIGURE 3 Plan view of spill-through abutment, floodplain, and channel.

Spill-Through Abutment

The spill-through abutment model, exhibited in the Figure 4, is comprised of four modular components as follows:

- Two 90-degree-curved embankment faces that make up the upstream and downstream corners of the spill-through abutment,
- Two 51- × 25-cm triangular prisms of variable length that make up the downstream and upstream faces of that are perpendicular to the direction of flow,
- One 15-cm-wide vertical abutment of variable length, and
- 51- × 25- × 15-cm triangular prism that extends from the abutment to the toe of the embankment.

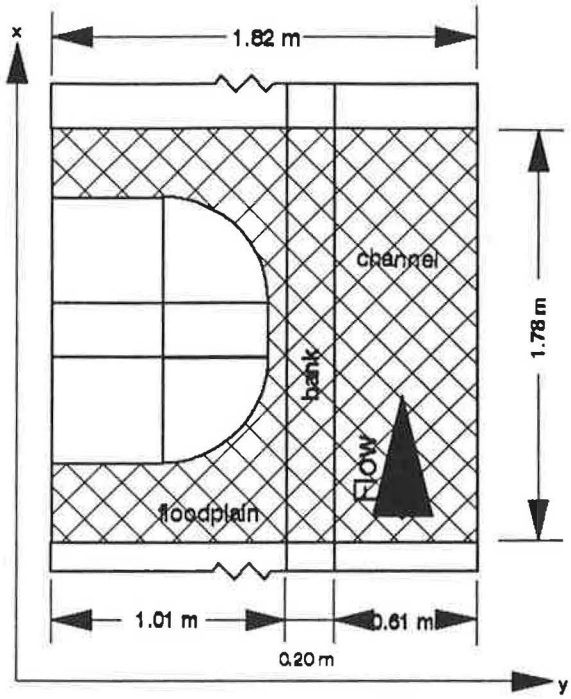

FIGURE 4 Profile view of spill-through abutment, floodplain, and channel.

These units are fastened together and anchored to the test section floor. The exposed surface of all the components are a mixture of fine sand and asphalt to simulate a concrete surface roughness. The spill-through abutment centerline was situated at the 8.12-m (26.63-ft) station from the reference datum at the flume tailbox.

As illustrated in the Figure 4, the dimensions of the spill-through abutment were as follows:

- Abutment length = variable, 13 to 51 cm (5 to 20 in.);
- Abutment width = 15 cm (6 in.);
- Embankment width = 117 cm (46 in.);
- Abutment height = 25 cm (10 in.); and
- Side slopes = 2:1 (horizontal:vertical).

Floodplain and Channel

The stream prototype is simulated as a floodplain and a channel in this study as displayed in Figures 3 and 4. The floodplain and channel were constructed from CDX fir plywood coated with a mixture of sand and asphalt. The spill-through abutment model was placed on the floodplain in the test section. The side slope of the channel was 2:1 (horizontal:vertical), and the channel height was 10 cm (4 in.). Within the test section where the spill-through abutment model was situated, both the floodplain and the channel were lined with riprap.

Riprap Lining

Riprap was modeled in the experiments by two sizes of uniformly graded gravel with D_{50}'s of 7.94 and 11.11 mm (0.31 and 0.41 in.). The smaller gravel represents the geometric mean size of the gravel that passed through the 9.5-mm sieve, was retained by the 6.3-mm sieve, and had a specific gravity of 2.702. The larger gravel passed through the 12.7-mm sieve was retained by the 9.5-mm sieve, and had a specific gravity of 2.709. Since the gravel bed had a thickness of 2.5 cm, two layers of gravel were used to make the riprap apron. Beneath the two layers of gravel is the sand- and asphalt-coated wood surface that was painted neon red in the expected area of failure. The observed area of failure from previous laboratory experiments was consistently at the toe of the embankment on the downstream side of the abutment centerline.

Experimental Plan

The objective of the physical modeling in this study was to simulate the threshold of movement of the gravel material used to protect the floodplain and channel in the vicinity of the spill-through abutment. The experiments were designed to identify the hydraulic conditions that precipitate incipient motion by the process of variation of the following hydraulic properties and model dimensions:

- Tailwater depth,
- Discharge,
- Abutment length,
- Bed slope, and
- Medium grain size, D_{50}, of the gravel.

Velocity is a function of the discharge, flow depth, and bed slope. Hence, it varies as a consequence of the modification to the aforementioned variables. Since the stability of the sediment depends on velocity and flow depth, the stability of the sediment can be modeled for a wide range of scenarios.

The procedure for approaching incipient motion is an iterative experimental process in which the aforementioned hydraulic properties were adjusted by small increments. Generally, when failure was accomplished, discharge was held constant and the tailwater depth, and thus the velocities, were decreased by small increments until incipient motion was "bracketed." By bracketing incipient motion, experiments simulated hydraulic conditions just before and just after the threshold of movement. Conversely, if the experiment did not achieve failure, the tailwater depth was decreased, and thus velocities were increased, by small increments until failure was attained.

Ultimately, the experiments that most closely replicated incipient motion compose the data from which a relationship can be developed. By eliminating the other experiments (i.e., experiments that were not considered to closely simulate incipient motion) from the data analysis, much of the data scatter can be minimized, thereby producing a better correlation.

Location of Data Measurement Stations

In the context of this study, average velocity is defined as a function of time, flow depth, and flow area, respectively, as follows:

- Average point-velocity measurements: orthogonal x- and y-component velocity measurements were made by the electromagnetic current meter at a rate of 10 Hz and averaged over a 30-sec period. These velocity readings were taken at depths of two-, six-, and eight-tenths of the depth and at the bed to give a complete representation of the velocity profile.
- Depth-averaged velocities: the aforementioned average point-velocity measurements taken at various depths at a given station can then be averaged to yield a depth-averaged velocity.
- Spatially averaged velocities: the average point velocity is taken at locations on the floodplain, channel, bank, and abutment to define the average cross-sectional velocities as well as represent the velocity distribution from the approach to the constriction to the exit sections, both with accuracy.

The spatially averaged, or average cross-sectional, velocity is computed for each transect (e.g., approach, centerline, failure, and exit). These velocities can be verified by using the continuity equation to compute the discharge at the cross section and compare it with the flow readings measured by the venturi meter. The general form of the equation would be

$$Q_{ci} = \sum_{j=1}^{n} V_j w_j d_j \tag{16}$$

where

Q_{ci} = computed discharge for Cross Section i [m³/sec (ft³/sec)];
V_j = depth-averaged velocity for Measuring Station j [m/sec (ft/sec)];

w_j = width of flow field represented by measured velocity, V_j [m (ft)]
$= y_{j+1} - y_{j-1}$,
y_j = transverse distance of measurement stations from flume wall [m (ft)]; and
d_j = measured depth of Station j [m (ft)]

Generally, more measuring stations in a transect yield computed flows that are much closer to the measured flow. The error in computed velocity-based flow to measured flow can be represented as follows:

$$\varepsilon_i = \frac{|Q_m - Q_{ci}|}{Q_m} \tag{17}$$

where Q_m equals flow measured by the venturi meter, in cubic meters (or feet) per second, and ε_i is the relative error of computed flow to measured flow.

These computations not only serve to produce averaged one-dimensional hydraulic properties (e.g., average velocity, average depth, and cross-sectional discharge), but also allow for quality assurance and quality control of the data-taking procedures and measuring instruments. Observations from the experiments indicate that accuracy (i.e., the minimization of relative error, ε_i) is highest for transects with more measurement stations and flow regimes resembling uniform flow. Generally, ε_i is less than 0.10 for the approach and contracted centerline sections.

From previous laboratory studies of spill-through abutments, it was observed that the failure zone occurs at the toe of the abutment slightly downstream of the centerline. Furthermore, it was learned tha the local average-point velocity at the failure zone approaches zero because of the turbulent flow that predominates in the flow region. The presence of the turbulent flow is accompanied by rotational flow. Because the measuring instruments can only measure the x- and y-directions, the x- and y-components of velocity that result from rotational flow in the x-y plane cancel each other out to yield an average velocity almost equal to zero.

Representative Discharges

Three different flows were simulated for all the abutment length and gravel sizes. Associated with the three flows are the depths ranging from shallow, medium, and deep flow depth in the floodplain. Generally, as abutment length (i.e., degree of flow obstruction) increased, the backwater effect increased for each of the flow scenarios. For the longest abutment length, the highest flows had to be decreased slightly because the abutment would have been overtopped. Typically, the three modeled flows in these experiments were 0.13, 0.20, and 0.25 m³/sec.

Observed Failure

Similar laboratory studies, as corroborated by this study, consistently developed failure zones located at the toe of the embankment just downstream of the abutment centerline as depicted in Figure 5. Figure 5 shows the typical progression of

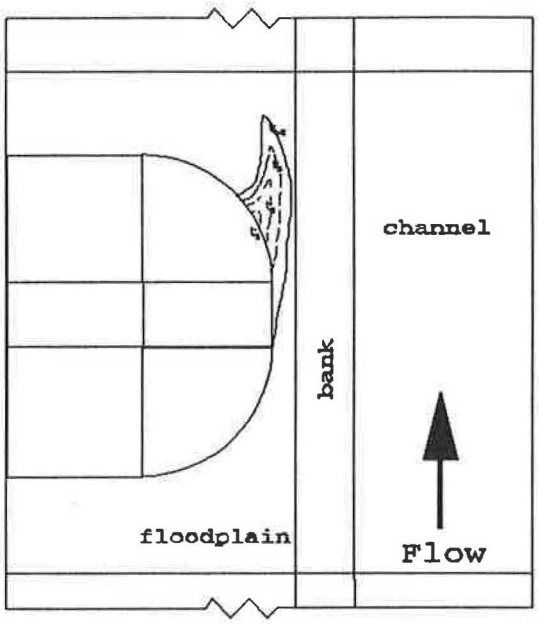

FIGURE 5 Typical riprap failure zone progression as a function of time.

the failure zone with respect to time. The failure zone reaches equilibrium at time, t_{eq} as depicted in Figure 5, which was typically 90 min to 2 hr in these experiments. Moreover, 24-hr experiments were conducted to verify that failure did not proliferate beyond the 4-hr simulation time of the experiments.

In the context of this study, failure was defined as the instantaneous moment when the unprotected surface was clearly exposed. As previously mentioned, a two-layer gravel apron was implemented. Hence, it could be argued that failure could vary for different thicknesses of gravel. Because incipient motion is such an extemporaneous phenomenon, the distinction between stability and failure is very fine. Furthermore, the unprotected surface experiences a change from a two-layer gravel cover to an exposed surface in a matter of seconds. As discussed earlier, incipient motion was approached by such small increments of variation of hydraulic parameters that the relativeness (or arbitrariness) of failure does not affect the hydraulic characteristics of incipient motion significantly.

ANALYSIS OF RESULTS

Surface Roughness Calibration

A series of experiments with just the channel and floodplain configuration were conducted to determine the Manning's roughness coefficient, n, fo the sandy asphalt surface. Manning's equation was rearranged to solve for n:

$$n = \frac{R^{2/3} S_e^{1/2}}{V} \tag{18}$$

where V is the measured depth-averaged velocity in meters (feet) per second, and R is the hydraulic radius (assumed to be depth in open channels) in meters (feet).

The energy gradeline was computed for evenly-spaced stations along longitudinal sections for three flow scenarios:

1. Bank-full flow (i.e., no flow in the floodplain),
2. Shallow floodplain flow, and
3. Deep floodplain flow.

The energy at each measurement station was computed using the energy equation

$$E = \frac{V^2}{2g} + d + z \tag{19}$$

where

V = depth-averaged velocity for the cross section,
d = average cross-sectional flow depth, and
z = vertical distance above reference datum.

From the energy computed in the longitudinal direction of flow, a slope of the energy gradeline can be determined. By applying this energy slope to Equation 18, an average Manning's n-value can be computed. These calibration experiments yielded a Manning's n-value of 0.0112 for the sandy paved wood surface of the floodplain and the channel. The laboratory-derived roughness coefficient is used throughout this study to quantify roughness for the sand and asphalt-coated wood.

Incipient Motion Results

As was the case with the previous spill-through abutment laboratory experiments, these experiments demonstrated that the failure zone develops at the toe of the abutment on the downstream side of the abutment centerline. The failure zone consistently precipitated where the flow separated, as illustrated in Figure 5, downstream of the abutment centerline. Regardless of the abutment length and proximity to the channel, the failure zone location remained constant. Even when the abutment toe was extended completely across the floodplain (i.e., 100 percent encroachment) adjacent to the channel, the gravel failed on the floodplain. The channel remained stable in all cases except when failure was excessive enough to spread to the channel bank. Since the focus of this study is to identify incipient motion (i.e., the moment that gravel begins to fail), the excessive failure that expanded to the channel bank is not relevant to the scope of this study.

Figure 6 illustrates the relationship between the stability of the particle (i.e., dimensionless shear stress) and the flow field (i.e., Froude number) in the constricted floodplain for previous spill-through abutment laboratory studies. Recall that previous laboratory studies represented particle stability with sediment number, N_{sc}, as a function of the relative roughness, D_{50}/d_{cc}, as exhibited in Figure 2. However, that relationship did not yield a good correlation. Figure 6 depicts a relationship that describes particle stability with Shields parameter is a better correlation.

Similarly, these laboratory experiments assume a relationship much like the one illustrated in Figure 6. By eliminating experimental data points that represent excessive failure (i.e., well beyond incipient motion) and non-failure well before incipient motion and considering the local (i.e., floodplain) hydraulic conditions, a good correlation between Shields parameter and the Froude number in the constricted floodplain can be developed, as illustrated in Figure 7.

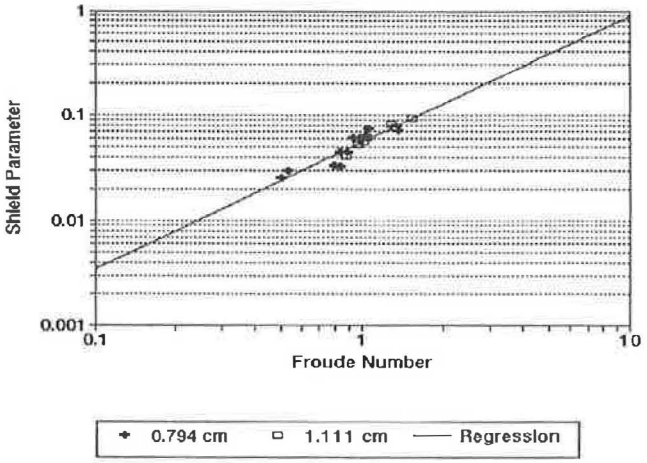

FIGURE 6 Relationship between Shields parameter and Froude number for spill-through abutments situated in floodplain with no channel.

A regression analysis yields a line, as depicted in Figure 7, that can be represented by the following equation:

$$\tau_* = 0.0556\ \mathrm{Fr}^{1.1997} \tag{20}$$

where τ_* is the Shields parameter, and Fr is the Froude number.

Substituting Equations 6 and 10, Equation 21 becomes

$$\frac{d_{fp}\, S_e}{D_{50}(S_g - 1)} = 0.0556\left(\frac{V_{fp}}{\sqrt{g d_{fp}}}\right)^{1.1997} \tag{21}$$

where

V_{fp} = depth-averaged velocity in the contracted floodplain (m/sec), and
d_{fp} = average floodplain flow depth in the contraction, in m.

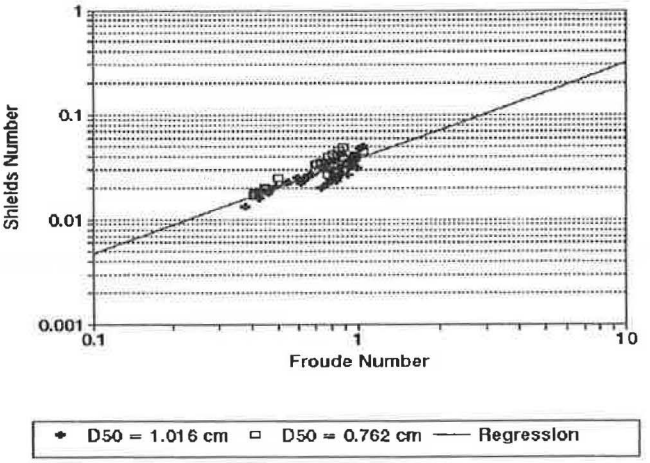

FIGURE 7 Relationship between Shields parameter and Froude number for contracted section of spill-through abutment floodplain.

Because of the limitations of these experiments, an energy slope, S_e, could not be measured accurately. The rapidly varied unsteady flow occurring at the toe of the abutment made accurate measurement very difficult Therefore, a theoretical approximation of the energy slope was made by rearranging Equation 19, which is a form of Manning's equation. The assumptions of Manning's equation is steady uniform flow, whereas these experiments demonstrated rapidly varied unsteady flow at the toe of the abutment and steady uniform flow everywhere else. However, the Manning equation is meant to provide a theoretical approximation of a hydraulic property that could not be measured experimentally. To obtain the Shields parameter, τ_*, from the experimental data, S_e was expressed in terms of the Manning equation, as follows:

$$S_e = \frac{V_{fp}^2 n^2}{d_{fp}^2} \tag{22}$$

Substituting into Equation 21 and rearranging to solve for D_{50} yields the following relationship:

$$D_{50} = \frac{17.988 n^2 V_{fp}^{0.8} g^{0.6} d_{fp}^{0.27}}{(S_g - 1)} \tag{23}$$

where D_{50} is the geometric mean grain size of the riprap in meters.

Because n is a function of D_{50}, either from experimental or theoretical derivation, it may be necessary to perform a few iterations before arriving at a solution for Equation 23. Furthermore, since Equation 23 defines the regression line that passes through the data points, the application of a factor of safety may be necessary. The selection of an appropriate factor of safety is left to the discretion of the designer. This linear relationship for floodplain with channel is comparable to the previous experimental studies of spill-through abutments with a floodplain and no channel. Since the data exhibited in Figure 7 represent local (i.e., spatially averaged in the floodplain only) hydraulic conditions and the previous experimental studies employed floodplains only, good agreement between the data from the two studies is the result, as demonstrated in Figure 8. Recall that the D_{50} sizes 0.794 and 1.111 cm were used for the experiments in this study, and 0.762 and 1.016 cm were used for the previous spill-through abutment experiments. The similarity shown in Figure 8 implies that a universal relationship can be developed to describe spill-through abutments in floodplains regardless of proximity to channels and varying abutment lengths, flows, flow depths, and velocities in the contraction.

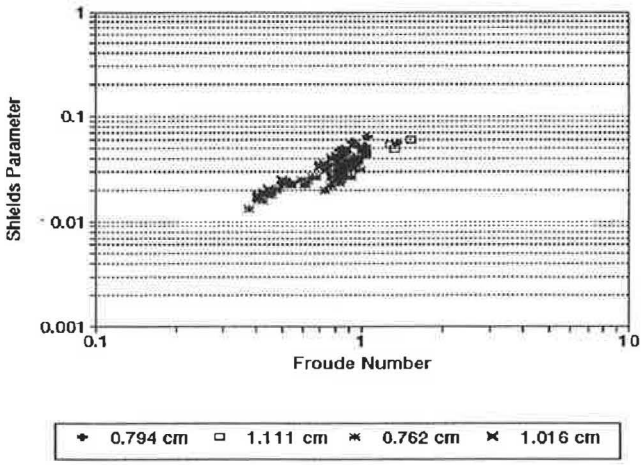

FIGURE 8 Comparison of spill-through abutments situated in floodplains near channels and spill-through abutments situated in floodplains with no channels.

CONCLUSIONS

This study established the following observations and relationships:

- The local Shields parameter correlates well with the local Froude number.
- There is good agreement between the results of this study and previous spill-through abutment studies in floodplains without a channel.
- A linear regression with a high coefficient of determination describes the experimental data points. From this linear relationship between the local Shields parameter and the local Froude number, the geometric mean grain size, D_{50}, of the riprap can be determined.
- Since failure always occurred on the floodplain initially, the stability of the riprap-lined channel is not undermined until failure is so excessive that it spreads to the channel.
- The failure zone always developed at the downstream side of the spill-through abutment toe regardless of the degree of encroachment or proximity of the spill-through abutment with respect to the channel. The location of the failure zone maintained consistency with previous studies.
- The progression of the failure zone is consistent for all the flow scenarios. Furthermore, the failure zone consistently reached equilibrium shortly after incipient motion.
- This study dovetails with previous spill-through abutment studies by proliferating the degree of encroachment on the floodplain. This study demonstrated that the design guidelines presented in this study is universally applicable for the entire range of encroachment simulated in this study and previous studies.
- The location of the spill-through abutment on the floodplain with respect to the channel did not affect the local hydraulic conditions that caused the riprap to fail at the abutment toe.
- Other references such as HEC-11 should be used for guidance in designing riprap revetment for the channel and bank, because this study revealed that the channel riprap stability was not affected by the proximity of the channel to the spill-through abutment. Therefore, the channel riprap can be treated as a separate design.

ACKNOWLEDGMENTS

The author would like to express his sincerest appreciation to Roy Trent of FHWA for his patience, guidance, and support throughout the course of the research project. The author extends gratitude to J. Sterling Jones of FHWA, whose guid-

ance, technical support, and expertise in hydraulic modeling contributed a great deal to efforts in this study.

The author also wishes to thank everyone at the National Highway Institute, especially Ilene Payne, for the opportunity to be part of the Grants for Research Fellowships (GRF) program. Her willingness to accommodate the author under the unusual circumstances of this GRF project is sincerely appreciated.

REFERENCES

1. Raudkivi, A. J. *Loose Boundary Hydraulics*. University of Auckland, New Zealand.
2. *Sedimentation Engineering*, (V. A. Vanoni, ed.) ASCE Manuals and Reports on Engineering Practice 54. ASCE, New York, 1975.
3. Shields, A. *Application of Similarity Principles and Turbulence Research to Bedload Movement*. California Institute of Technology, Pasadena, 1936 (English translation by W. P. Ott and J. C. van Uchelon).
4. Isbash, S. V. Construction of Dams by Depositing Rock on Running Water. *Trans. 2nd Congress on Large Dams*, Vol. 5, Washington, D.C., 1936, pp. 123–135.
5. Pagán-Ortiz, J. E. *Stability of Rock Riprap for Protection at the Toe of Abutments Located at the Floodplain*. FHWA, U.S. Department of Transportation, 1991.
6. *Design of Riprap Revetment*. Hydraulic Engineering Circular 11; FHWA-IP-89-016. FHWA, U.S. Department of Transportation, 1989.